Residual Stresses in High-Velocity Oxy-Fuel Metallic Coatings

T.C. TOTEMEIER, R.N. WRIGHT, and W.D. SWANK

X-ray based residual stress measurements were made on type 316 stainless steel and Fe_3Al coatings that were high-velocity oxy-fuel (HVOF) sprayed onto low-carbon and stainless steel substrates. Nominal coating thicknesses varied from 250 to 1500 μm. The effect of HVOF spray particle velocity on residual stress and deposition efficiency was assessed by preparing coatings at three different torch chamber pressures. The effect of substrate thickness on residual stress was determined by spraying coatings onto thick (6.4 mm) and thin (1.4 mm) substrates. Residual stresses were compressive for both coating materials and increased in magnitude with spray velocity. For coatings applied to thick substrates, near-surface residual stresses were essentially constant with increasing coating thickness. Differences in thermal expansion coefficient between low-carbon and stainless steels led to a 180 MPa difference in residual stress for Fe_3Al coatings. Deposition efficiency for both materials is maximized at an intermediate (~600 m/s) velocity. Considerations for X-ray measurement of residual stresses in HVOF coatings are also presented.

I. INTRODUCTION

THERMAL spray coatings are increasingly used for surface protection, primarily against high-temperature corrosion and wear. Coatings are commonly applied to hot section gas turbine components,[1] to midspan dampers on fan and compressor blades in aero turbines engines,[2] and are being investigated for use in advanced fossil energy plants.[3,4,5] In all cases, the longevity and durability of the coating are of paramount importance to its primary function of protecting the substrate component. Cracking or spallation of the coating compromises its essential function, and may lead to shortened component life compared to an uncoated condition.[2,6] It is therefore critical to understand factors that may lead to premature coating failure, in addition to simply measuring its resistance to a particular aggressive environment.

Residual stresses have been shown to play an important role in the cracking, adhesion, and spallation behavior of coatings.[2,7–10] In addition, residual stresses induced in the substrate by the coating process can also play a role in determining the overall component life.[2] Residual stresses in thermally sprayed coatings can be considered as the sum of three components: a tensile quench stress arising from the solidification and rapid cooling of individual spray particles upon impact with the much cooler substrate, a compressive peening stress imparted by impact of high-velocity spray particles, and a thermal mismatch stress incurred during cooling of the coating-substrate couple from the deposition temperature. The sign of the thermal mismatch stress will depend on the relative thermal expansion coefficients (CTEs) of the coating and substrate.

Residual stresses in thermal spray coatings have received considerable attention in the literature. Several different techniques have been used for measurement, all with intrinsic advantages and disadvantages; comprehensive reviews are given in References 11 and 12. To summarize, residual stress measurement techniques can be divided into three categories: measurement of crystallographic lattice parameters using X-ray diffraction (XRD) or neutron diffraction,[13–17] methods that relate the curvature of as-sprayed coating-substrate couples to stress in the coating and substrate,[3,5,18–21] and techniques that monitor changes in substrate strain upon layer-by-layer removal of the coating.[22] Lattice parameter methods directly measure coating strain (which can be related to stress), but require knowledge of coating physical constants and expensive instrumentation. Curvature-based methods are simple, but rely on analytical or numerical models (with necessary assumptions) to calculate coating and substrate stresses. Material removal methods permit determination of the residual stress variation through the thickness of the coating and substrate, but involve relatively time-consuming sample preparation and again rely on models to relate measured substrate strains to coating stresses.

Residual stress measurement has primarily been performed on plasma-sprayed ceramic coatings, since these find extensive industrial application as thermal barriers on gas turbine blades. For these coatings, quench and thermal mismatch stresses dominate the net coating residual stress due to the high temperature and low velocity of plasma spray particles and the large CTE mismatch between the ceramic coating and (typically) metal substrate.[9,23,24] The magnitude of the quench stress has been found to depend on intersplat bonding and microcracking within individual splats. Poor bonding and microcracking act to decrease coating stresses by reducing the net coating modulus—typical modulus values for yttria-stabilized zirconia are around 45 GPa,[25] only 20 pct of the bulk value.[26]

In contrast, peening stresses typically dominate in high-velocity, oxy-fuel (HVOF) coatings, due to higher spray particle velocities (up to 1000 m/s, compared to around 100 m/s for plasma spray) and lower temperatures (1500 °C to 1800 °C, compared to 2000 °C to 3000 °C for plasma spray).[12] In addition, HVOF coatings are typically metals or cermets with better CTE match to the substrate. Due to the large peening contribution, residual coating stresses in HVOF coatings are usually compressive, although some authors have reported tensile stresses.[2,22]

T.C. TOTEMEIER, Staff Engineer, R.N. WRIGHT, Department Manager, and W.D. SWANK, Advisory Engineer, are with the Idaho National Engineering and Environmental Laboratory (INEEL), Idaho Falls, ID 83415. Contact e-mail: totetc@inel.gov

Manuscript submitted June 30, 2003.

The effects of HVOF spray parameters on the characteristics of Fe_3Al and FeAl intermetallic coatings have been studied,[3,5,27] including effects on residual coating stresses. Higher spray particle velocities produced coatings with more compressive residual stresses, higher hardness, and decreased fractions of oxide and porosity. The changes in coating characteristics were related to increased peening effects of higher-velocity particles. There were difficulties, however, in relating curvature measurements of coating-substrate couples to actual coating stresses on thick, nonbending substrates. Similar effects of HVOF spray parameters have been reported for other material and spray systems,[18,28–30] although spray particle characteristics are frequently not quantified.

The aims of the research reported in this article are twofold: to investigate the effects of HVOF spray parameters on spray particle characteristics, deposition efficiency, and residual coating stresses; and to study the use of XRD techniques for residual stress measurement in HVOF coatings. Two coating materials were examined—Fe_3Al (to extend and clarify the previous work) and AISI type 316 stainless steel. Three different spray conditions were investigated for each material; the spray particle characteristics (size distribution, velocity, and temperature) and relative deposition efficiency were assessed for each material and spray condition. The XRD-based residual stress measurements were made for each material and spray condition on a series of coatings with varied thickness sprayed onto thin (deforming) and thick (nondeforming) substrates. In addition to reporting the results of these measurements, this article discusses important factors in the X-ray measurement of residual stresses in HVOF coatings.

II. EXPERIMENTAL PROCEDURES

A. *Coating Preparation and Spray Particle Characterization*

The variation of spray particle characteristics and residual coating stresses with HVOF spray parameters was investigated for two coating materials: AISI type 316 stainless steel (Tafa 1236F) and an Fe_3Al-based alloy. Both alloys were obtained commercially in powder form: the 316 SS powder from Praxair-Tafa (Concord, MA), and the Fe_3Al alloy (designated FAS) from Ametek Specialty Metal Products (Eighty Four, PA). The nominal composition of FAS is Fe-16Al-2Cr (wt pct). Both powders were screened to −270 mesh; the median sizes of the screened powders are given in Table I.

A JP5000 HVOF spray gun (Praxair-Tafa) with a 0.10-m barrel was used to prepare coatings from the feedstock powder at a fixed standoff distance of 3.55 m. The coatings were built up layer by layer using a raster deposition scheme with a 0.20 m/s transverse velocity. Each pass in front of the torch produced an approximately 45-μm-thick layer. Coatings were applied to rectangular substrates that were either AISI 1020 low-carbon steel or type 316 stainless steel. Substrate dimensions were either $76 \times 12.5 \times 1.4$ mm^3 or $76 \times 12.5 \times 6.4$ mm^3. The thin substrates were used for curvature measurements (presented in a subsequent article), while the thick substrates were intended to resist deformation resulting from the coating application. Both sides of all substrates were grit blasted with alumina prior to coating.

Table I shows relevant coating parameters and spray particle characteristics investigated. Kerosene ($C_{10}H_{20}$) was used as the fuel with a pure oxygen gas oxidant. The principal variable was the torch chamber pressure, which was adjusted by changing the input flow rates of the fuel and oxidant while maintaining an equivalence ratio of one (a stoichiometric mixture). The effect of changing torch chamber pressure on the temperature and velocity characteristics of the thermal spray particles was quantified using an integrated laser Doppler velocimeter and high-speed two-color pyrometer. The estimated (1σ) measurement uncertainties are 5 pct for particle temperature and less than 5 m/s for particle velocity.[31,32] Coatings for residual stress characterization using X-ray diffraction were produced using both powders at each torch pressure.

The relative deposition efficiency of the different spray parameters was assessed from the coating thicknesses produced for each condition after an equal number of passes of the substrate in front of the torch. The deposition of the thickest coating produced was assigned a deposition efficiency of one; the deposition efficiencies for other conditions were computed as the ratio of the coating thickness for a given condition to that of the thickest coating.

B. *Residual Stress Measurement*

Coating residual stresses were measured using standard d *vs* $\sin^2 \psi$ XRD techniques, as described in Reference 33. Measurements were made on a Bruker AXS diffractometer (Madison, WI) with Cr K_α radiation. For 316 SS coatings, the (220) peak at $2\theta = 129$ deg was measured; for Fe_3Al coatings, the (211) peak at $2\theta = 150$ deg was measured. The Bruker-supplied STRESS application was used to calculate residual stresses from peak positions. Young's moduli for 316 SS and Fe_3Al were taken as 200[34] and 140 GPa,[3] respectively. Crystallographic anisotropy factors for 316 SS and Fe_3Al were taken as 1.72 and 1.49, respectively.[35] The

Table I. HVOF Spray Conditions and Particle Characteristics

Powder Material	Median Powder Particle Size (μm)	Oxygen Flow (L/min)*	Kerosene Flow (L/h)	Chamber Gage Pressure (kPa)	Spray Particle Temperature (°C)	Spray Particle Velocity (m/s)
316 SS	20 to 38	520	16.7	350	1320	520
		700	22.7	510	1310	610
		820	26.5	614	1300	640
Fe_3Al	20 to 38	520	16.7	350	1650	560
		700	22.7	510	1680	600
		820	26.5	614	1650	620

*At standard temperature and pressure.

lattice positions of 316 SS and Fe_3Al feedstock powders were measured in identical conditions as the coatings; the powder data was used in the STRESS application to correct the coating data for instrumental effects. The application-computed error of the measurements due to fitting of the d *vs* $\sin^2\psi$ plots varied from sample to sample but was generally on the order of 20 MPa.

Residual stress measurements were made on the coating surface along the 12.5-mm direction of the coating-substrate couple, *i.e.*, parallel to the short axis of the original substrate. Measurements of stresses in both short and long axes were performed on several specimens to confirm the biaxial stress state; these were equal within the stated measurement accuracy.

Stresses were generally measured on coating surfaces from which 75 to 100 μm had been removed by grinding with 600-grit paper and polishing to a 1-μm finish. Surface removal was performed in order to provide a flat X-ray measurement surface and avoid the effects of surface roughness on the measured stresses. The potential effect of the grinding and polishing procedure on residual stress was assessed by measuring stresses on annealed 316 SS specimens before and after surface removal—in both cases, no residual stresses were observed. This is considered a worst case for generation of surface stress by the polishing procedure, and hence, no effect of grinding and polishing on measured coating residual stresses in the as-sprayed condition is expected. Residual stress measurements were made on the as-coated surfaces of a series of Fe_3Al specimens for comparison with results obtained on polished surfaces.

The repeatability of residual stress measurements on a single specimen was assessed for both 316 SS and Fe_3Al coatings and always found to be within the fitting error computed by the STRESS application (~20 MPa). The variation of residual stress with position within a coating-substrate couple was assessed by measuring stresses on five separate specimens removed from the same couple. While the stress variation, ~40 MPa, was greater than observed for repeated measurements on a single specimen, no trend in stress with position within the couple was observed.

Table II is the matrix of all conditions for which residual coating stresses were measured. For 316 SS coatings applied to 316 SS substrates, stresses were measured for all variations of particle velocity, substrate thickness, and coating thickness, while stresses in Fe_3Al coatings were measured in a more limited range of conditions. The variation of residual stress with coating thickness was investigated primarily by measuring stresses on multiple coatings whose thicknesses varied from approximately 250 to 1500 μm; five coatings with varied thickness in this range were produced for each combination of powder and chamber pressure. The thickness variation in stress was also characterized by repeated measurements on a single Fe_3Al coating (applied on a 6.4-mm-thick substrate) from which successive 200-μm layers were removed.

III. RESULTS

A. *Spray Particle Characteristics and Deposition Efficiency*

The HVOF spray particle temperature and velocity characteristics are listed in Table I. Figure 1 graphically shows the variation of these parameters with torch chamber pressure. Particle temperatures for both powders are essentially constant with varying chamber pressure at the fixed equivalence ratio, as observed in previous work on INCONEL* 718.[32]

*INCONEL is a trademark of INCO Alloys International, Huntington Woods, WV.

The observed temperatures for the Fe_3Al powder, however, were considerably greater than for 316 SS, 1650 °C to 1680 °C compared to 1300 °C to 1320 °C.

Sound, adherent coatings were produced in all conditions. The microstructures of Fe_3Al coatings were presented in Reference 5; further details of the microstructure and properties of the 316 SS coatings will be presented in a future publication. Relative deposition efficiencies obtained for the varied spray parameters are shown in Figure 2, in which efficiency is plotted as a function of particle velocity. Particle velocity is plotted instead of torch chamber pressure since this is believed to represent a more fundamental variable. Coatings prepared at identical velocity and temperature and similar powder particle sizes should result in similar properties, regardless of the particular HVOF torch used, whereas the relationship between chamber pressure and velocity will depend on equipment and other environmental factors. Both 316 SS and Fe_3Al show a maximum deposition efficiency at an intermediate particle velocity (approximately 600 m/s) with reduced efficiency at lower and higher velocities.

Table II. XRD Residual Stress Measurement Matrix

Coating Material	Substrate Material	Substrate Thickness (mm)	Spray Particle Velocity (m/s)	Nominal Coating Thicknesses (μm)
316 SS	316 SS	1.4	520	250 to 1500
			610	
			640	
316 SS	316 SS	6.4	520	250 to 1500
			610	
			640	
Fe_3Al	AISI 1020	1.4	620	250 to 1500
Fe_3Al	AISI 1020	6.4	560	250 to 1500
			600	
			620	
Fe_3Al	316 SS	6.4	620	250 to 1500

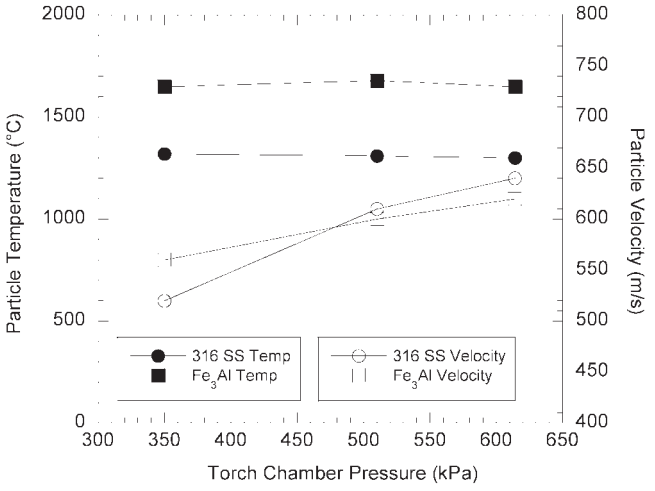

Fig. 1—Spray particle velocity and temperature *vs* torch chamber pressure for 316 SS and Fe_3Al powders.

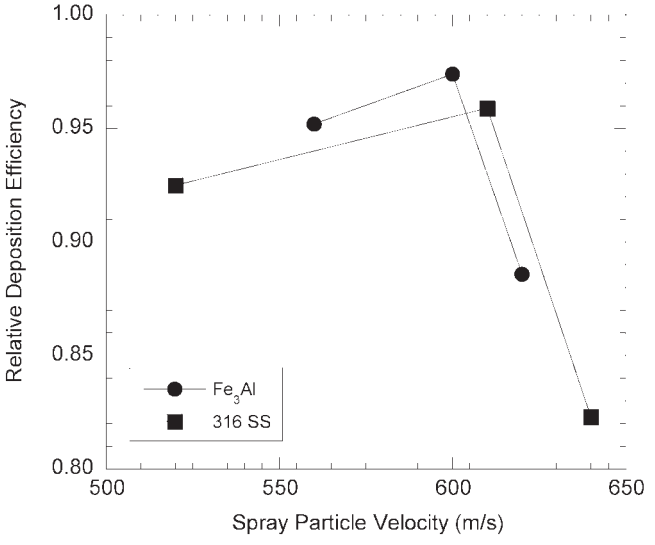

Fig. 2—Relative coating deposition efficiency as a function of spray particle velocity for 316 SS and Fe_3Al coatings.

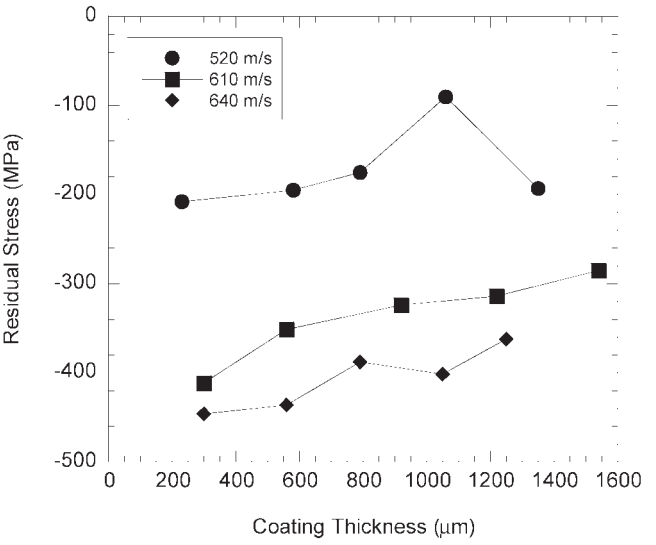

Fig. 3—XRD-measured residual stresses for 316 SS coatings applied to 1.4-mm-thick 316 SS substrates.

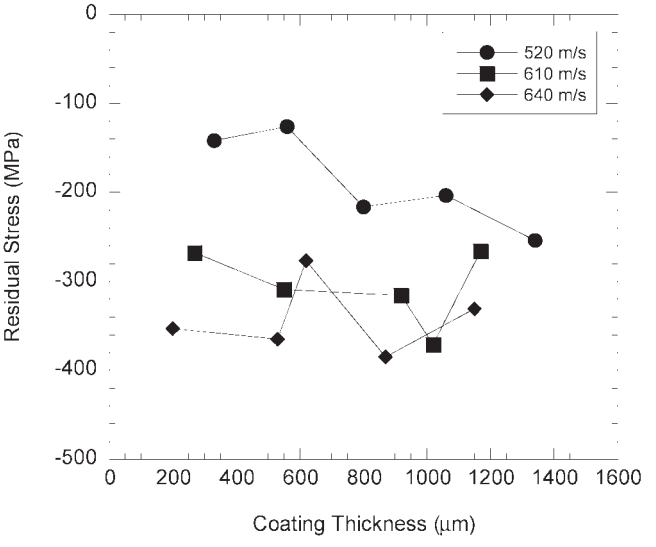

Fig. 4—XRD-measured residual stresses for 316 SS coatings applied to 6.4-mm-thick 316 SS substrates.

B. *Residual Stresses*

The results of XRD residual stress measurements of 316 SS coatings applied to thin (1.4 mm) and thick (6.4 mm) 316 SS substrates are shown in Figures 3 and 4, respectively. Stresses are presented as a function of coating thickness for three spray particle velocities. As noted previously, each data point represents a measurement on a unique coating-substrate couple. Significant scatter is present, especially for coatings on thick substrates, greatly exceeding the fitting error and scatter observed for multiple specimens from a single couple.

For 316 SS coatings on thin substrates, residual stresses become less compressive with increasing coating thickness; this trend is observed for all particle velocities. In contrast, for thick substrates, residual stresses are relatively constant with coating thickness for the two higher particle velocities, and stresses for coatings sprayed at the 520 m/s particle velocity become more compressive. Despite the scatter, it is clear that residual stresses become more compressive with increasing spray velocity. The effect is more pronounced for coatings on thin substrates, and for both substrates, there is a larger increase going from 520 to 610 m/s than from 610 to 640 m/s.

Figure 5 shows residual stresses for Fe_3Al coatings. Data are shown for all conditions investigated: three particle velocities on thick low-carbon steel substrates, and the highest velocity on a thick stainless steel substrate and a thin low-carbon steel substrate. The effect of surface condition is shown by data for the 620 m/s velocity taken on unpolished coating surfaces. For Fe_3Al coatings, the residual stresses are essentially constant with coating thickness. Significant scatter is again observed. Residual stresses for

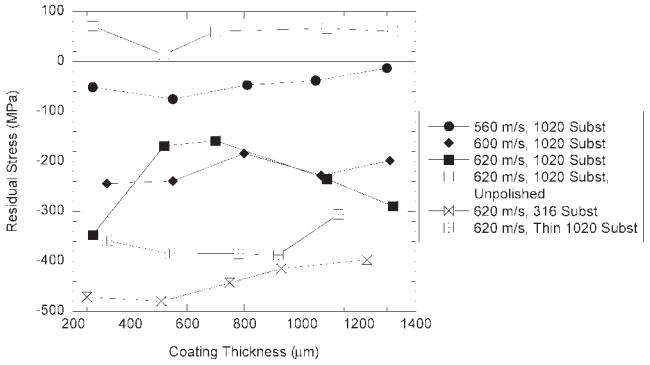

Fig. 5—XRD-measured residual stresses for Fe_3Al coatings applied to thick (6.4 mm) and thin (1.4 mm) 1020 steel and 316 SS substrates. Also shown are data obtained on unpolished coating surfaces.

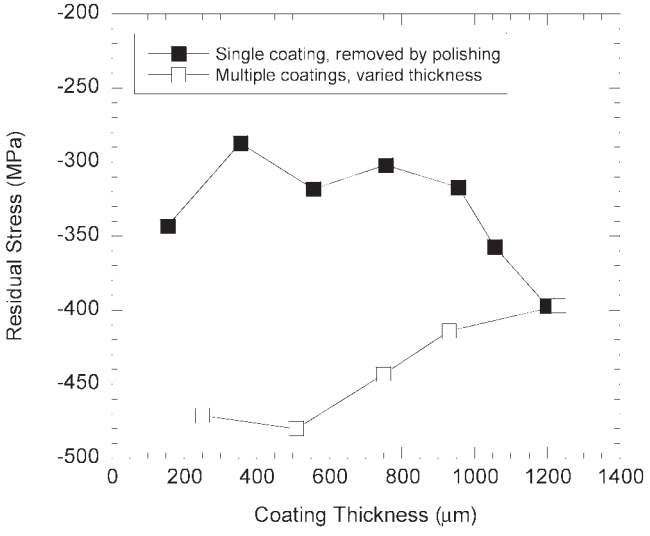

Fig. 6—Through-thickness residual stress distribution in an Fe_3Al coating on a thick 316 SS substrate obtained by repeated measurements on a single specimen after incremental layer removal. Thickness variation data obtained on multiple specimens are shown for comparison.

coatings on thick, low-carbon steel substrates become more compressive with increasing particle velocity, and coatings applied to 316 SS substrates have significantly higher stresses than those applied to low-carbon steel. The marked effect of surface condition is demonstrated by the tensile stresses measured on unpolished surfaces.

Figure 6 compares the variation of residual stress in Fe_3Al with coating thickness (316 SS substrate, 620 m/s particle velocity) measured by layer removal on a single specimen with the variation of surface stress with thickness measured on multiple specimens. For the layer removal specimen, measured residual stresses are plotted *vs* the remaining coating thickness to facilitate comparison with the multiple specimen data. The data points at 1250 μm are the same measurement; the 1250-μm-thick coating was then polished down in steps. The two data sets appear to show opposite trends: the layer removal data show more compressive stress with increasing coating thickness (less material removed), while the multiple specimen data show less compressive stress with increasing thickness.

IV. DISCUSSION

A. *Effect of Spray Parameters on Particle Characteristics and Deposition Efficiency*

As shown in Figure 1, torch chamber pressure has a strong influence on spray particle velocity for both 316 SS and Fe_3Al powders, but essentially no effect on spray particle temperature. Spray particle velocities increase 23 pct for 316 SS and 10 pct for Fe_3Al with an increase in pressure from 350 to 614 kPa. These observations are in agreement with findings reported by other researchers.[3,5,17,31,36] All report linear increases in particle velocity with chamber pressure over pressures ranging from 400 to 1000 kPa. Reported particle velocities vary from approximately 300 to 800 m/s, again in good agreement with the current results. As previously noted,[32,36] the acceleration of a spray particle (and hence its final velocity) in a HVOF spray nozzle is dependent on the dynamic gas pressure acting on it, which in turn is dependent on the combustion chamber pressure.

Particle temperature, however, is dependent on the temperature of the combustion gas flow and the residence time of the particle in the gas. Swank *et al.*[31] found that the gas temperature is relatively insensitive to chamber pressure, but strongly dependent on flame temperature, which is in turn a function of equivalence ratio. Particle residence time will decrease with chamber pressure as the velocity increases, but the effect is not significant relative to changes in combustion gas flame temperature.

The high temperatures observed for Fe_3Al spray particles are believed to at least partly result from rapid oxidation of Al on the particle surfaces during spraying in air.[5] The heat and radiation emitted in this reaction may give rise to anomalously high pyrometer temperature readings. The observation of a significant fraction of unmelted particles in the coating microstructure[5] indicates that particle temperatures are closer to the melting point of Fe_3Al (1540 °C).

Few researchers have reported the effects of HVOF spray parameters on the deposition efficiency, although this is an important parameter in industrial applications, particularly spraying of expensive feedstock powders. Measurement of the effect of particle velocity on the relative deposition efficiency for 316 SS and Fe_3Al powders was made possible by the use of constant powder feed characteristics and torch passes across the varied particle velocities. Hence, the coating thickness provides a relative measure of deposition efficiency. It is notable that a maximum in deposition efficiency is obtained for both powders at an intermediate velocity; this is somewhat contrary to the intuitive belief that the "sticking percentage" of impacting particles will continually increase with velocity, thereby resulting in continually increasing deposition efficiency. Better sticking of particles at higher impacting velocities has been observed for cold spraying[37] as well as HVOF spraying.[30] Lower velocity particles that are partially molten do not have sufficient kinetic energy to deform on impact and adhere to the substrate. The increase in efficiency going from low to intermediate velocities in the current study is attributed to this mechanism. At higher velocities, however, the deposition efficiency decreases. This is attributed to loss of material due to "splashing" of molten or nearly-molten particles upon high velocity impact. Splashing of particles at high velocities has been reported by Hackett and Settles[38] and Wright *et al.*[39]

B. *Residual Stress Measurement*

This article presents the results of a systematic study of residual stresses in HVOF metallic coatings measured using XRD, similar to a study performed by Matejicek *et al.*[16] on plasma-sprayed coatings. The XRD technique has been shown to be an effective means of measuring residual stresses in HVOF coatings, and it is worth noting some specific findings that arose in the experimental procedure development. First, the results obtained confirm that the stress state in HVOF coatings is purely biaxial. Equal stresses on the coating surface were measured in two perpendicular directions, and no shear stresses were indicated in the d *vs* $\sin^2\psi$ plots; overlapping straight lines were observed at positive and negative ψ values. The importance of surface preparation is shown by the results of unpolished *vs* polished specimens. Results obtained on unpolished surfaces indicate tensile coating stresses, when in fact essentially all of the coating is strongly in compression (refer to further subsequent discussion).

Significant scatter in the XRD results is apparent in Figures 3 through 5, which makes clear observations of trends difficult. The scatter appears to be between separate coating-substrate couples, rather than intrinsic to the XRD measurement or within a given couple. The scatter is present despite the fact that all coatings were sprayed in the same session using identical setup and powder. The results suggest that the degree of variability from coating to coating be carefully addressed for applications in which the magnitude of the residual stress is a critical performance factor. Due to the involved nature of XRD residual stress measurement, it would be expedient to use a simpler method (e.g., curvature measurement) to assess the variability of coating stresses.

C. *Variation in Residual Stress with Coating and Substrate Thickness*

The progressive deposition model of Tsui and Clyne[40] provides a good framework for interpreting the "theoretical" variation of residual coating stresses with thickness. Their model calculates the distribution of coating and substrate stresses for a given system assuming that the coating is applied in layers, and that a "deposition stress" is associated with each newly added layer. The deposition stress is constant for a given set of coating parameters: powder type and size; spray particle temperature and velocity. Although the model was presented in the context of plasma-sprayed coatings, it is equally valid for HVOF coatings, albeit with a compressive deposition stress. For an infinitely thick substrate, this model predicts a constant residual stress with increasing coating thickness, since the deposition stress in each layer is not relieved by substrate deformation and the formation of curvature. In the case of thinner, deformable substrates, however, stresses measured on the coating surface become less compressive with increasing coating thickness, due to progressive deformation as the coating is applied.

The results of the present study on 316 SS coatings are in agreement with the predicted trends. Stresses measured on the surface of coatings applied to thin substrates become less compressive with increasing thickness, while stresses for thick substrates are relatively constant (with the exception of coatings applied at 520 m/s). For Fe_3Al, residual stresses on both thick and thin substrates appear to be constant with increasing coating thickness. The trends in residual stress with thickness agree with the findings of Matejicek et al.,[16] who measured surface stresses in plasma-sprayed Mo. They observed nearly constant tensile residual stresses with increasing thickness. Kesler *et al.*[13] report a slight decrease in tensile residual stresses with increasing coating thickness for neutron diffraction measurements, also of plasma-sprayed Mo, again in agreement with the progressive model.

The relative magnitudes of stresses on thin and thick substrates, however, do not agree with predictions of the progressive model. For a constant deposition stress, measured coating stresses for thin substrates are expected to be less compressive than for thick substrates, due to stress relaxation by substrate deformation. The opposite is observed for both 316 SS and Fe_3Al coatings—stresses on thin substrates are consistently more compressive than those on thick substrates. The source of this discrepancy is currently unknown—stresses estimated from curvature of coating-thin substrate couples are lower than those measured using XRD. A complete presentation of the curvature data and models used to derive coating and substrate stresses from curvature is planned for a future publication.

With respect to the through-thickness variation in residual stress shown in Figure 6, the progressive model predicts that the two trends shown in Figure 6 should overlap; *i.e.*, the measured surface stresses after layer removal should agree with the stress measured on the surface of a coating sprayed to the same thickness. Again, the source of the discrepancy between theoretical predictions and measurement is unknown, but might be due to plasticity in the coating or substrate; the progressive model assumes elastic behavior. In any case, it is apparent that XRD may not be an ideal technique for determining through-thickness variations in residual stress.

One aspect of the through-thickness variation of residual stress for HVOF coatings clearly revealed in this study is the marked difference in residual stress at the coating surface (in the last layer deposited) and in the coating as a whole. The measurements made on unpolished surfaces of Fe_3Al coatings indicate that the last coating layer is in a state of tension rather than compression. For Cr K_α radiation, the thickness of the diffracting volume (90 pct contribution to the diffracted beam) for the (211) peak is approximately 12 μm. The sampling depth is entirely within the last layer deposited, and some reduction in stress magnitude due to free-surface effects is expected. Unlike the remainder of the coating, the last layer is not peened by the impact of additional depositing particles, and hence the stress measured is tensile, more representative of the quench stress. This marked change in stress after removal of 75 μm of coating is a further indication of the magnitude of the peening effect in HVOF coatings. Similar near-tensile residual stresses at the very surface of HVOF coatings have been observed using layer removal methods.[22]

D. *Spray Parameter Effects on Residual Stress*

Figure 7 summarizes residual coating stresses as a function of spray particle velocity for 316 SS and Fe_3Al. The stress values shown are the mean of stresses at all thicknesses for each condition; the data were averaged, assuming constant stress with thickness, to reduce scatter resulting from specimen-

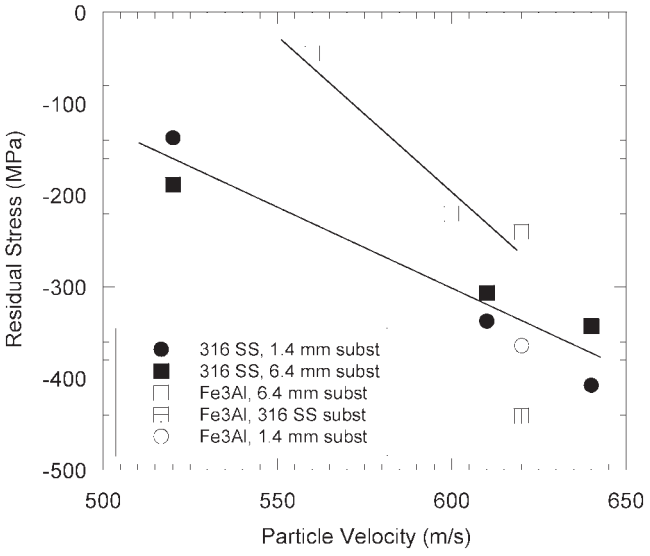

Fig. 7—Variation of residual stress for 316 SS and Fe_3Al coatings with spray particle velocity. Data shown represent mean values of coatings with varied thickness.

to-specimen variations. Trendlines are shown to demark the different coatings. Both materials show an apparently linear increase in compressive residual stress with spray particle velocity. As stated previously, the stress increase results from increased peening effects imparted by higher-velocity particles. In this study, the magnitude of the peening effect appears to be linearly dependent on the particle velocity (or momentum, given the constant powder size) rather than kinetic energy (square of velocity), as observed by Kuroda *et al.*[17] Given the limited data, it is difficult to say with certainty which parameter (momentum or energy) controls the magnitude of the peening effect; further tests are planned in this area.

The effect of substrate material on residual stresses in Fe_3Al coatings is also clearly shown in Figure 7. The mean stress value for Fe_3Al on 1020 steel is −240 MPa, compared to −420 MPa on 316 SS. The difference results from the difference in CTE for the two substrate materials. The mean CTE for 1020 steel from the deposition temperature (~200 °C) to room temperature is 12.7 ppm/°C, similar to that for the Fe_3Al coating in the same range[3] (12.5 ppm °C); hence, there is little CTE mismatch contribution to the final residual stress. The CTE for 316 SS is considerably higher, 17.5 ppm/°C, leading to a compressive CTE mismatch stress of −175 MPa (for biaxial conditions and a thick substrate), which agrees well with the measured difference of −180 MPa. It is worthwhile noting that the reported CTE value for bulk, wrought Fe_3Al from room temperature to 200 °C is 16 ppm/°C;[41] hence, predictions based on bulk values rather than coating values would predict little CTE mismatch stress for 316 SS. This example reinforces the importance of measuring physical properties of coatings rather than assuming bulk values.

V. CONCLUSIONS

This article presented the results of a study of residual stresses in HVOF-sprayed 316 SS and Fe_3Al metallic coatings. The effects of coating and substrate thickness, spray particle velocity, and substrate material were assessed and the following conclusions reached.

1. Increasing torch chamber pressure results in increasing spray particle velocity with little change in spray particle temperature.
2. Relative deposition efficiencies are maximized at an intermediate particle velocity, 610 m/s for 316 SS and 600 m/s for Fe_3Al. The reduction at higher particle velocity is attributed to increased "splashing" of the impacting droplet.
3. Near-surface residual stresses in 316 SS coatings on thin substrates become slightly less compressive with increasing coating thickness; stresses in 316 SS coatings on thick substrates and all Fe_3Al coatings were independent of coating thickness.
4. Due to an increased peening effect, increasing spray particle velocity leads to more compressive residual stresses for both coating materials.
5. Residual stresses measured on the surface of unpolished Fe_3Al coatings were tensile, reflecting the lack of peening in the last layer of coating deposited.
6. Differences in CTE values between low-carbon (1020) and 316 SS substrates lead to a 180 MPa difference in residual stresses for Fe_3Al coatings applied at a 620 m/s spray particle velocity.

ACKNOWLEDGMENTS

The authors acknowledge the assistance of D.C. Haggard with preparation of coatings and T.C. Morris with metallography. This work was supported by the United States Department of Energy, Office of Fossil Energy, under Department of Energy Idaho Operations Office Contract No. DE-AC07-99ID13727.

REFERENCES

1. G.W. Goward: *Mater. Sci. Technol.*, 1986, vol. 2, pp. 194-200.
2. L. Pejryd, J. Wigren, D.J. Greving, J.R. Shadley, and E.F. Rybicki: *J. Thermal Spray Technol.*, 1995, vol. 4, pp. 268-74.
3. T.C. Totemeier, R.N. Wright, and W.D. Swank: *Metall. Mater. Trans. A*, 2003, vol. 34A, pp. 2223-231.
4. M. Kramer, O. Degirmen, A.J. Thom, and M. Akinc: Paper presented at *15th Annual Conf. on Fossil Energy Materials*, Knoxville, TN, 2001.
5. T.C. Totemeier, R.N. Wright, and W.D. Swank: *J. Thermal Spray Technol.*, 2002, vol. 11, pp. 400-08.
6. T.C. Totemeier and J.E. King: *Metall. Mater. Trans. A*, 1996, vol. 27A, pp. 353-62.
7. R.T.R. McGrann, D.J. Greving, J.R. Shadley, E.F. Rybicki, T.L. Kruecke, and B.E. Bodger: *Surface Coatings Technol.*, 1998, vols. 108–109, pp. 59-64.
8. S.J. Howard, Y.C. Tsui, and T.W. Clyne: in *1994 Thermal Spray Industrial Applications*, C.C. Berndt and S. Sampath, eds., ASM INTERNATIONAL, Materials Park, OH, 1994, pp. 703-08.
9. S. Kuroda, T. Fukushima, and S. Kitahara: in *Thermal Spray: International Advances in Coatings Technology*, C.C. Berndt, ed., ASM INTERNATIONAL, Materials Park, OH, 1992, pp. 903-09.
10. D.J. Greving, J.R. Shadley, and E.F. Rybicki: *J. Thermal Spray Technol.*, 1994, vol. 3, pp. 371-78.
11. T.W. Clyne and S.C. Gill: *J. Thermal Spray Technol.*, 1996, vol. 5, pp. 401-18.
12. S. Kuroda: in *Thermal Spray: Meeting the Challenges of the 21st Century*, C. Coddet, ed., ASM INTERNATIONAL, Materials Park, OH, 1998, pp. 539-50.

13. O. Kesler, J. Matejicek, S. Sampath, S. Suresh, T. Gnaeupel-Herold, P.C. Brand, and H.J. Prask: *Mater. Sci. Eng. A*, 1998, vol. A257, pp. 215-24.
14. I. Iordanova and K.S. Forcey: *Surface Coatings Technol*., 1997, vol. 91, pp. 174-82.
15. J. Matejicek, S. Sampath, P.C. Brand, and H.J. Prask: in *Thermal Spray: A United Forum for Scientific and Technological Advances*, C.C. Berndt, ed., ASM INTERNATIONAL, Materials Park, OH, 1997, pp. 861-66.
16. J. Matejicek, S. Sampath, and J. Dubsky: *J. Thermal Spray Technol*., 1998, vol. 7, pp. 489-96.
17. S. Kuroda, Y. Tashiro, H. Yumoto, S. Taira, H. Fukanuma, and S. Tobe: *J. Thermal Spray Technol*., 2001, vol. 10, pp. 367-74.
18. R. Knight and R.W. Smith: in *Thermal Spray Coatings: Research, Design, and Applications*, C.C. Berndt and T.F. Bernecki, eds., ASM INTERNATIONAL, Materials Park, OH, 1993, pp. 607-12.
19. S.C. Gill and T.W. Clyne: *Thin Solid Films*, 1994, vol. 250, pp. 172-80.
20. W.D. Swank, R.A. Gavalya, J.K. Wright, and R.N. Wright: in *Thermal Spray: Surface Engineering via Applied Research*, C.C. Berndt, ed., ASM INTERNATIONAL, Materials Park, OH, 2000, pp. 363-69.
21. O. Kesler, M. Finot, S. Suresh, and S. Sampath: *Acta Mater*., 1997, vol. 45, pp. 3123-34.
22. D.J. Greving, E.F. Rybicki, and J.R. Shadley: *J. Thermal Spray Technol*., 1994, vol. 3, pp. 379-88.
23. J. Matejicek, S. Sampath, P.C. Brand, and H.J. Prask: *Acta Mater*., 1999, vol. 47, pp. 607-17.
24. J. Matejicek and S. Sampath: *Acta Mater*., 2001, vol. 49, pp. 1993-99.
25. E.F. Rybicki, J.R. Shadley, X. Xiong, and D.J. Greving: *J. Thermal Spray Technol*., 1995, vol. 4, pp. 377-84.
26. J.W. Adams, R. Ruh, and K.S. Mazdiyasn: *J. Am. Ceram. Soc*., 1997, vol. 80, pp. 903-08.
27. T.C. Totemeier, R.N. Wright, and W.D. Swank: *Intermetallics*, in press, 2004.
28. Y. Itoh, M. Saitoh, and M. Tamura: *J. Eng. Gas Turbines and Power*, 2000, vol. 122, pp. 43-49.
29. S. Kuroda, Y. Tashiro, H. Yumoto, S. Taira, and H. Fukanuma: in *Thermal Spray: Meeting the Challenges of the 21st Century*, C. Coddet, ed., ASM INTERNATIONAL, Materials Park, OH, 1998, pp. 569-74.
30. C.-J. Li and Y.-Y. Wang: *J. Thermal Spray Technol*., 2002, vol. 11, pp. 523-29.
31. W.D. Swank, J.R. Fincke, D.C. Haggard, and G. Irons: in *Thermal Spray Industrial Applications*, C.C. Berndt and S. Sampath, eds., ASM INTERNATIONAL, Materials Park, OH, 1994, pp. 307-12.
32. W.D. Swank, J.R. Fincke, D.C. Haggard, G. Irons, and R. Bullock: in *Thermal Spray Industrial Applications*, C.C. Berndt and S. Sampath, eds., ASM INTERNATIONAL, Materials Park, OH, 1994, pp. 319-24.
33. I.C. Noyan and J.B. Cohen: *Residual Stress—Measurement by Diffraction and Interpretation*, Springer-Verlag, New York, NY, 1987.
34. S.H. Crandall, N.C. Dahl, and T.J. Lardner: *An Introduction to the Mechanics of Solids*, 2nd ed., McGraw-Hill, New York, NY, 1978.
35. *Stress User's Manual*, Bruker AXS GmbH, Karlsruhe, Germany, 1999.
36. T.C. Hanson, C.M. Hackett, and G.S. Settles: *J. Thermal Spray Technol*., 2002, vol. 11, pp. 75-85.
37. R.C. Dykhuizen, M.F. Smith, D.L. Gilmore, R.A. Neiser, X. Jiang, and S. Sampath: *J. Thermal Spray Technol*., 1999, vol. 8, pp. 559-64.
38. C.M. Hackett and G.S. Settles: in *Thermal Spray: Practical Solutions for Engineering Problems*, C.C. Berndt, ed., ASM INTERNATIONAL, Materials Park, OH, 1996, pp. 665-73.
39. R.N. Wright, J.R. Fincke, W.D. Swank, and D.C. Haggard: in *Thermal Spray: Practical Solutions for Engineering Problems*, C.C. Berndt, ed., ASM INTERNATIONAL, Materials Park, OH, 1996, pp. 511-16.
40. Y.C. Tsui and T.W. Clyne: *Thin Solid Films*, 1997, vol. 306, pp. 23-33.
41. J.H. Schneibel: in *Processing, Properties, and Applications of Iron Aluminides*, J.H. Schneibel and M.A. Crimp, eds., TMS, Warrendale, PA, 1994, pp. 329-42.